Electronic Spectra of Single-Crystal Maleonitriledithiolate Complexes of Iridium(I): $[Ir(CO)_2mnt]$ TBA ($mnt \equiv [S_2C_2(CN)_2]^{2-}$; $TBA \equiv [(C_4H_9)_4N]^+$)

U. Riedl and G. Gliemann

Institut für Physikalische und Theoretische Chemie, Universität Regensburg, Regensburg, FRG

Z. Naturforsch. **44a**, 1057–1062 (1989); received July 18, 1989

The polarized optical absorption and emission (spectra, decay times) of single-crystal $[Ir(CO)_2mnt]$ TBA at temperatures $2\,K \leqq T \lesssim 295\,K$ and homogeneous magnetic fields $0 \leqq H \leqq 6\,T$ are reported. The highly resolved spectra show 0–0 transitions with vibrational satellites and phonon side bands. Applied magnetic fields yield no effect on the emission. The lowest excited electronic states can be assigned to the spin-orbit components A'_1, B'_1, and B'_2 of the charge transfer triplet $^3A_2$ (symmetry C_{2v}).

Introduction

Transition metal complexes with maleonitriledithiolate ($=mnt \equiv [S_2C_2(CN)_2]^{2-}$) ligands and Ni(II), Pd(II), Pt(II) as central ions have been studied comprehensively by spectroscopic methods in the last years [1–15]. The said complexes exhibit interesting properties, e.g. intense color, relatively high stability, and a strong delocalization of their π-electron systems. Little information is available on corresponding iridium(I) complexes. Since the bis(maleonitriledithiolate) complex of iridium(I) seems to be not stable, iridium(I) complexes with mixed ligand systems such as $[Ir(CO)_2mnt]^-$ have been used for experimental studies. Recently results of NMR, IR and electronic absorption spectroscopy with liquid solutions (room temperature) and glassy solutions ($T \sim 77\,K$) of this compound have been reported [16].

The purpose of this paper is to yield more insight into the electronic structure of maleonitriledithiolate complexes of iridium(I). To this end we describe the results of highly resolved and polarized optical absorption and emission spectra of single-crystal $[Ir(CO)_2mnt]$ TBA (TBA = tetrabutylammonium). External parameters are the temperature ($2\,K \leqq T \lesssim 295\,K$) and applied magnetic fields ($0 \leqq H \leqq 6\,T$). On the basis of the experimental results an energy level diagram for the lowest excited states of the $[Ir(CO)_2mnt]^-$ ion is proposed.

Reprint requests to Prof. Dr. G. Gliemann, Institut für Physikalische und Theoretische Chemie, Universität Regensburg, D-8400 Regensburg.

Experimental

The compound $[Ir(CO)_2mnt]$ TBA was prepared according to [17]. Application of the method described in [16] has been found to be ineffective because of the low yield and the poor purity of the product. Light-brownish single crystals of the compound (size $(\sim 0.1 \times 0.2 \times 0.05)\,mm^3$) have been obtained from acetonitril solutions at room temperature.

For the measurement of the polarized luminescence the cryostat of a superconducting magnet of Oxford Instruments (SM 4) yielding magnetic fields up to 6 T has been used, cf. [18]. Excitation was by the 364 nm line of an argon ion laser (Coherent innova 90). The emitted light was selected by a Spex double grating monochromator (type 1404) and detected by an EMI S 20 photomultiplier. The apparatus for the lifetime measurement has been described in [19]. The measurements of the polarized absorption were performed with a special spectrometer for micro crystals [20].

Results

Figure 1 shows the absorption spectrum of $[Ir(CO)_2mnt]$ TBA dissolved in acetonitrile at room temperature. The spectrum in the low-energy range ($\bar{\nu} \lesssim 40 \cdot 10^3\,cm^{-1}$) is composed of a strong band A and three shoulders B, C, D at the red flank of A, cf. Table 1.

For single-crystal $[Ir(CO)_2mnt]$ TBA at $T = 10\,K$ an additional weak absorption between $\bar{\nu} \sim 18\,000\,cm^{-1}$

0932-0784 / 89 / 1100-1057 $ 01.30/0. – Please order a reprint rather than making your own copy.

and the shoulder D has been detected, cf. Figure 2. The corresponding spectrum is distinctly structured and starts at its low-energy side with a peak I ($\bar{\nu} = 18\,310\ cm^{-1}$, $\varepsilon \sim 15\ M^{-1}\ cm^{-1}$). Peak I is followed by a system of seven additional peaks of lower extinction at energies between $\bar{\nu} = 18\,501\ cm^{-1}$ and $19\,396\ cm^{-1}$. This part of the spectrum is repeated three times at increasing energy, cf. also Table 2. The most intense peaks I, II, III, IV of the four sections have half-widths of about $\Delta\bar{\nu} \sim 90\ cm^{-1}$ and yield a progression of $\bar{\nu} = 1260\,(\pm 20)\ cm^{-1}$.

Table 1. Absorption spectral data for an acetonitrile solution of $[Ir(CO)_2mnt]TBA$ at $T = 298$ K; $c = 2.4 \times 10^{-3}$ M.

Band	Energy of the band $[10^3\ cm^{-1}]$	Extinction coefficient[a] $\varepsilon\,[M^{-1}\ cm^{-1}]$
A	34.24	8200
B	31.5	~5500
C	29.5	~3000
D	27.5	~1000

[a] Total extinction coefficient at the wavenumber given in the second column.

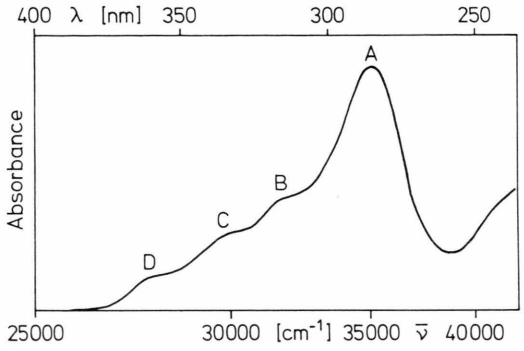

Fig. 1. Electronic absorption spectrum of $[Ir(CO)_2mnt]TBA$ dissolved in acetonitrile [$c = 2.4 \times 10^{-3}$ M] at room temperature.

The low-energy absorption exhibits a polarization ratio $\varepsilon_{\parallel}/\varepsilon_{\perp}$ of about 2, with $\varepsilon_{\parallel}$ and $\varepsilon_{\perp}$ the extinction coefficients for the polarizations $\mathbf{E} \parallel \mathbf{A}$ and $\mathbf{E} \perp \mathbf{A}$, respectively. **A** is defined by the direction of extinction of the single crystal. The energies of the peak maxima are independent of the orientation of **E**.

At room temperature acetonitrile solutions of $[Ir(CO)_2mnt]TBA$ show no luminescence, whereas the crystalline compound yields an extremely weak and very broad emission band between $\bar{\nu} = 14\,200\ cm^{-1}$ and $18\,500\ cm^{-1}$. With decreasing temperature the emission of single crystalline $[Ir(CO)_2mnt]TBA$ gains intensity, and at $T \sim 160$ K the emission exhibits a weak structure, which becomes more and more pronounced as the temperature is lowered further. At $T < 20$ K a fine structure is resolved. This is dominated by a progression of intense lines I′, II′, III′, and IV′ separated by $\Delta\bar{\nu} \sim 1460\,(\pm 30)\ cm^{-1}$, cf. Figure 3. These lines have half-widths of about $25\ cm^{-1}$. At their low-energy side the lines I′, II′, III′ and IV′ are accompanied by similarly structured systems of relatively weak emission peaks. Figure 4 shows the low energy section of the corresponding system of line I′ on a larger scale. The wave-numbers of the peaks and their distances from line I′ are summarized in Table 3.

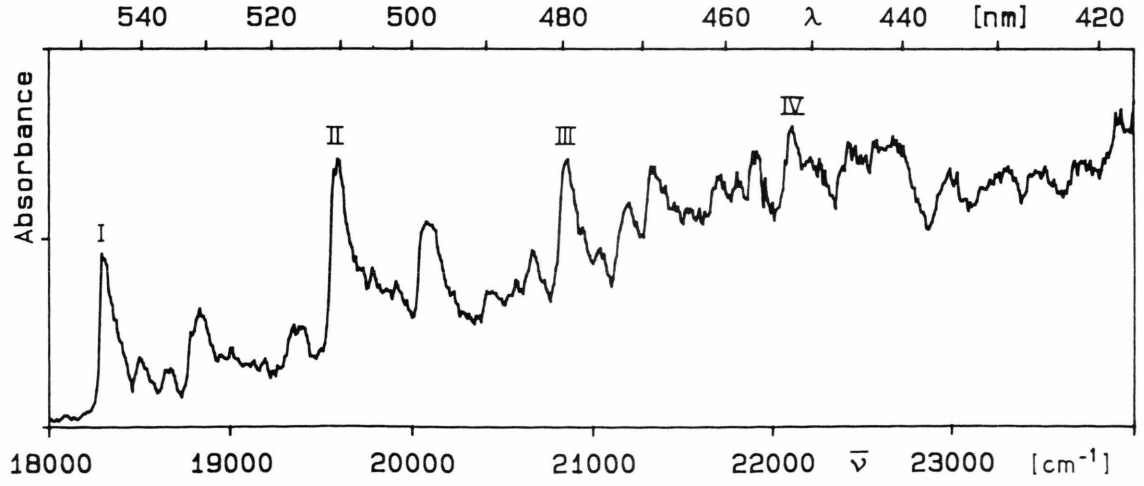

Fig. 2. $\mathbf{E} \perp \mathbf{A}$ polarized absorption spectrum of single-crystal $[Ir(CO)_2mnt]TBA$ at $T = 10$ K.

Within the limits of experimental error ($\Delta\bar{\nu} \sim 10\ cm^{-1}$) the lines II′, III′, and IV′ and their assigned systems of peaks show the same energy separations.

At $T = 2$ K the emission of single crystalline [Ir(CO)$_2$mnt]TBA is polarized with an intensity ratio $I_{\parallel}/I_{\perp}$ of about 2, which equals the corresponding extinction ratio of the polarized absorption spectra at low temperatures.

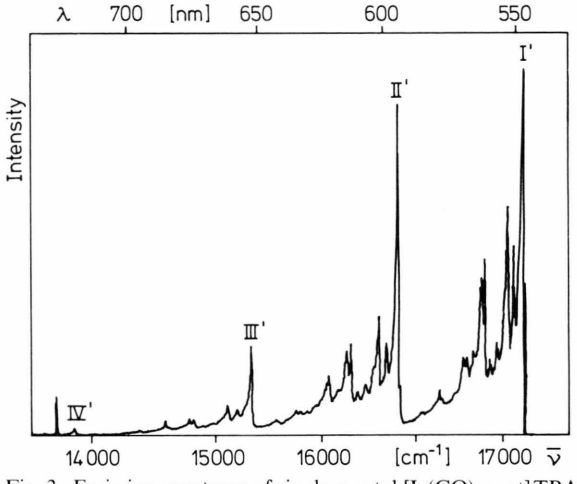

Fig. 3. Emission spectrum of single-crystal [Ir(CO)$_2$mnt]TBA at $T = 2$ K ($\lambda_{ex} = 364$ nm).

Table 2. Absorption spectral data of single-crystal [Ir(CO)$_2$mnt]TBA at $T = 10$ K; Polarization $\mathbf{E} \perp \mathbf{A}$.

Peak energies [cm^{-1}]	Energy distances from the peaks I, II, III, IV, respectively [cm^{-1}]	Energy distances between the peaks I, II, III, IV [cm^{-1}]
18 310 (I)		
18 501	191	
18 656	346	
18 787	477	
18 835	525	
19 014	704	
19 169	859	
19 396	1086	
19 586 (II)		1276
19 765	179	
19 920	334	
20 052	466	
20 099	513	
20 266	680	
20 421	835	
20 660	1074	
20 851 (III)		1265
21 030	179	
21 173	322	
21 316	465	
21 364	513	
21 531	680	
21 698	847	
21 924	1073	
22 091 (IV)		1240
22 246	155	
22 462	371	
22 592	501	

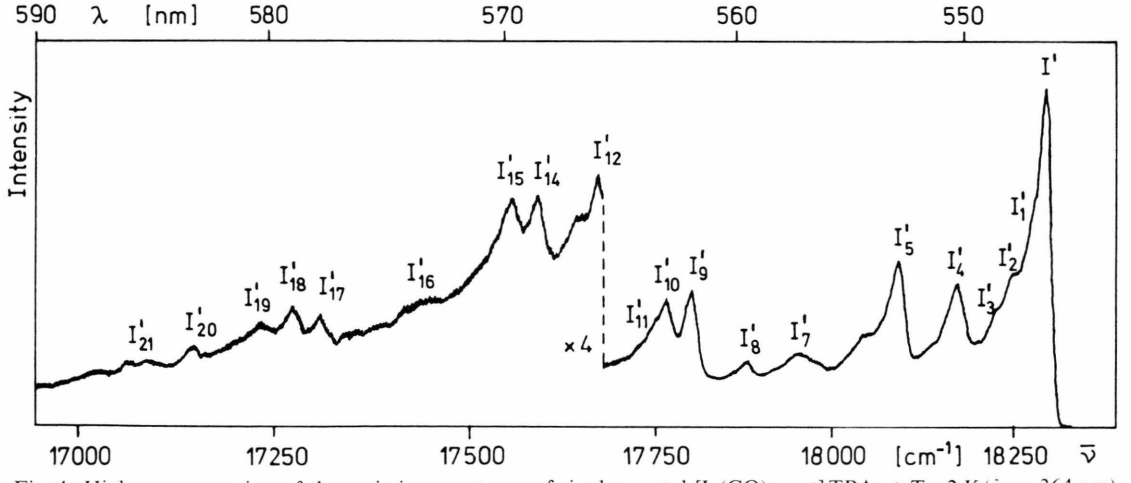

Fig. 4. High energy section of the emission spectrum of single-crystal [Ir(CO)$_2$mnt]TBA at $T = 2$ K ($\lambda_{ex} = 364$ nm).

Table 3. Emission spectral data of single-crystal $[Ir(CO)_2mnt]TBA$ for the low energy section at $T=2$ K.

Peak energies [cm^{-1}]	Energy distances from line I′ [cm^{-1}]
18 284 (I′)	–
18 278	6
18 238	46
18 224	60
18 162	122
18 099	185
18 037	247
17 948	336
17 876	408
17 803	481
17 761	523
17 743	541
17 670	614
17 639	645
17 590	694
17 556	728
17 436	848
17 310	974
17 271	1013
17 229	1055
17 137	1147
17 064	1220

At $T=2$ K the emission lines I′ and I'_5 exhibit a mono-exponential decay yielding a lifetime of $\tau \sim 310$ μs independent of the polarization. Increase of the temperature to $T=5$ K reduces the lifetime of these lines to ~ 100 μs. At higher temperatures the intensities were too low for decay experiments. The other peaks I'_i, $i \neq 5$, show bi-exponential decay curves, indicating decreasing lifetimes with decreasing energies of the peaks.

Homogeneous magnetic fields **H** with field strengths $0 \leqq H \leqq 6$ T and orientations $\mathbf{H} \parallel \mathbf{A}$ and $\mathbf{H} \perp \mathbf{A}$ yield no effects on the emission (peak energies, intensities, lifetimes).

Discussion

A crystal-structure analysis of $[Ir(CO)_2mnt]TBA$ is not available as yet. Recently, the crystal structure of the similar compound $[Ir(CO)_2mnt]_2MV$ (MV = methyl viologen) has been determined by Eisenberg et al. [21]. The space group is $C2/c$ with square planar Ir(I) complex anions. In the following it is assumed that for $[Ir(CO)_2mnt]TBA$ the central d^8-ion with its nearest neighbors form a planar frame of C_{2v} symmetry as shown schematically in Figure 5. A MO diagram of

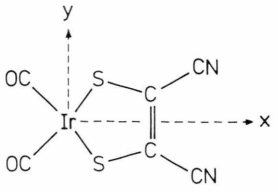

Fig. 5. Schematic structure of $[Ir(CO)_2mnt]TBA$ and molecular axes.

the $[Ir(CO)_2mnt]^-$ ion can be constructed according to the results for $[Ni(mnt)_2]^{2-}$ [22] and $[Pt(mnt)_2]^{2-}$ [15]. The latter complex ions have $b_1(\pi, xz)$ hybrids as HOMO's which are composed of π-orbitals of the mnt ligands and of metal d_{xz}-orbitals. The LUMO's of the Ni(II) and the Pt(II) complexes, however, are different. For $[Ni(mnt)_2]^{2-}$ a $b_2(xy)$ state could be established as LUMO, whereas the ligand state $a_2(\pi^*)$ has higher energy. In the $[Pt(mnt)_2]^{2-}$ ion the energy order of these states is inverted and $a_2(\pi^*)$ is the LUMO. Because of the similarity of the central ions Ir(I) and Pt(II) the MO diagram of $[Ir(CO)_2mnt]^-$ should be similar to that of $[Pt(mnt)_2]^{2-}$, but the differences of the metal valency and of the ligand systems have to be taken into account. If the ligand field strengths in both complexes are assumed to be comparable, it can be concluded from the different metal valencies that the energy splitting of the d-orbitals in $[Ir(CO)_2mnt]^-$ is smaller than in $[Pt(mnt)_2]^{2-}$. As a consequence, in $[Ir(CO)_2mnt]^-$ the d-state $b_2(xy)$ can be shifted below the ligand state $a_2(\pi^*)$ and then it functions as LUMO. In the following it will be investigated, whether the experimental results for $[Ir(CO)_2mnt]^-$ are compatible with the proposed energy order of $b_1(\pi, xz)$ and $b_2(xy)$ as HOMO and LUMO, respectively.

An electronic transition $b_1^2 \rightarrow b_1^1 b_2^1$ yields the many electron states $^1A_2$ and $^3A_2$ which can be classified in the double group C'_{2v} as $A'_2(^1A_2)$ and A'_1, B'_1, $B'_2(^3A_2)$, respectively. The expected polarizations of the electric-dipole allowed transitions between the triplet states and the ground electronic state $A'_1(^1A_1)$ are shown in Figure 6a.

Applied homogeneous magnetic fields $\mathbf{H} \parallel \mathbf{x}$ and $\mathbf{H} \perp \mathbf{x}$ reduce the symmetry of the system to C_2 and C_s, respectively. The magnetic-field induced couplings and the resulting polarizations of the allowed transitions are given in Figs. 6 b, c, d.

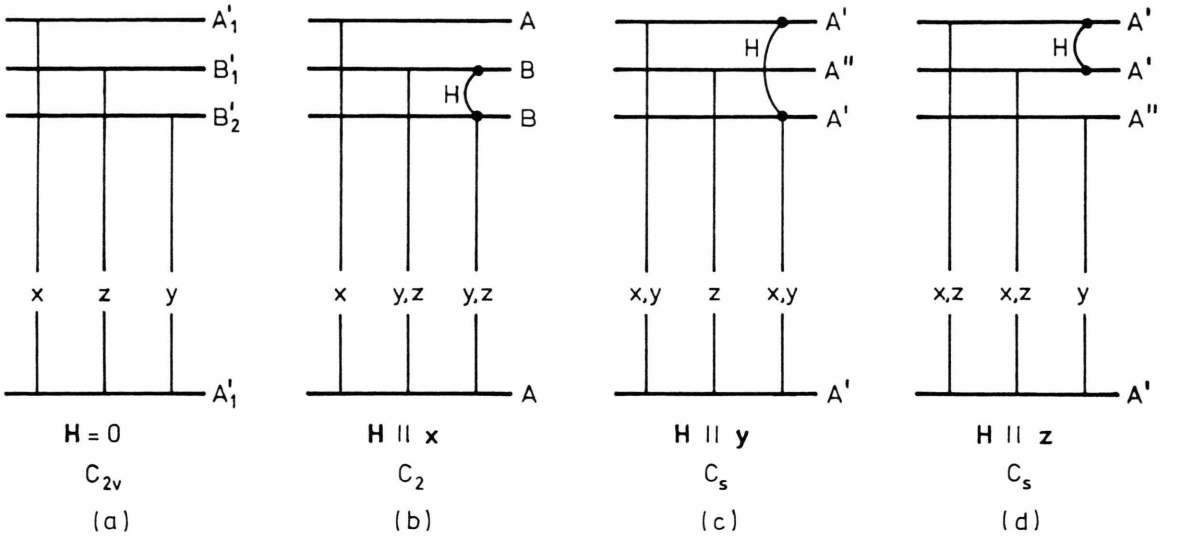

Fig. 6. Schematic energy level diagram and electric dipole transitions between the ground electronic state and the lowest excited states of $[Ir(CO)_2mnt]^-$. (a) without magnetic field, (b, c, d) with homogeneous magnetic fields of different orientations.

With regard to its large extinction coefficient, spectral position, and half-width, the absorption band A of the solution spectrum (cf. Fig. 1) is due to a singlet-singlet π–π^* transition of the ligand mnt. The energy of the π–π^* transition of the free ligand ($\bar{\nu}$ = 27 027 cm^{-1}, ε = 5500 $M^{-1}\,cm^{-1}$) is increased in the complex owing to the interaction of the ligand states with metal states of corresponding symmetry. The absorption band D and the two shoulders C and B can be assigned to the singlet-singlet charge transfer transition $^1A_1 \rightarrow {}^1A_2$ and to two superimposed vibrations ($\bar{\nu}_{vib} \sim 205\ cm^{-1}$ and $\sim 410\ cm^{-1}$), respectively, cf. [16].

The weak absorption of the single crystals observed between $\bar{\nu}$ = 18 310 cm^{-1} and 22 600 cm^{-1} at low temperatures can be assigned to the singlet-triplet CT transition $^1A_1 \rightarrow {}^3A_2$. If spin-orbit coupling is effective this transition is electric dipole allowed with polarizations $\mathbf{E} \parallel \mathbf{x}$ ($A'_1 \rightarrow A'_1$), $\mathbf{E} \parallel \mathbf{y}$ ($A'_1 \rightarrow B'_2$), and $\mathbf{E} \parallel \mathbf{z}$ ($A'_1 \rightarrow B'_1$), cf. Figure 6a. Since reports on the crystal structure of $[Ir(CO)_2mnt]TBA$ are not available, a definite assignment of the molecular axes x, y, z to the **A** axis cannot be established. However, from the experimental result that only the intensities but not the spectral positions of the low-energy absorption peaks depend on the polarization, the following conclusions can be drawn: (i) the spin-orbit splitting of the $^3A_2$ is distinctly smaller than the half-width of the peaks ($\sim 90\ cm^{-1}$). Therefore, the energy order and the separation of the spin-orbit components A'_1, B'_1 and B'_2 cannot be determined from the absorption spectra. (ii) In the crystal the complex ions $[Ir(CO)_2mnt]^-$ are ordered with regard to their orientation. That is compatible with the structural data for crystalline $[Ir(CO)_2mnt]_2MV$, showing a parallel arrangement of the square planar Ir(I) complex anions [21].

The distinct 1260 cm^{-1} progression of the dominant bands I, II, III, and IV in Fig. 2 results from a superposition of the totally symmetric C=C vibration of the ligand mnt [16]. For the peaks between the dominant bands probably other vibrations of the complex ion are responsible, but a definite assignment cannot be given because corresponding raman data are not available.

Since band I′ of the emission spectrum (cf. Figs. 3 and 4) has the same energy as the absorption band I, it can be concluded that both bands belong to 0–0 transitions between the ground electronic state and the lowest triplet states A'_1, B'_1, B'_2 ($^3A_2$). Furthermore, the emission spectrum exhibits a similar fine structure as the low-energy absorption spectrum. The dominating 1460 cm^{-1} progression in the emission spectrum can also be assigned to the C=C vibration of the mnt ligand, although its energy is distinctly higher than in the absorption spectrum ($\Delta\bar{\nu} \sim$ 1260 cm^{-1}). This discrepancy is a consequence of the partial removal of a bonding π electron from the mnt ligand by excitation. The low intensity peaks between

the emission bands I′, II′, III′, and IV′ are probably due to the coupling of other complex vibrations and of phonons. The polarization properties of the emission agree with the above mentioned conclusion that the spin-orbit splitting of the $^3A_2$ components is small. From the emission spectra it can be concluded that the splitting does not exceed a few wavenumbers.

The large value of the emission lifetime at low temperatures ($\tau \sim 310$ μs) confirms the triplet-singlet character of the emission process. Raise of the temperature reduces the lifetime as a result of an enhancement of the non-radiative deactivations.

The lack of magnetic field effects on the emission follows straightforwardly from Figure 6. Since radiative deactivations of the triplet components A'_1, B'_1, and B'_2 are allowed already at zero field, the magnetic-field induced coupling of these states is expected to yield no measureable effect on the emission properties at $H \leqq 6$ T.

Acknowledgement

This research has been supported by the Deutsche Forschungsgemeinschaft and the Fonds der Chemischen Industrie. We thank R. Eisenberg for providing information prior to publication.

[1] J. A. McCleverty, Progr. Inorg. Chem. **10,** 49 (1968).
[2] R. Eisenberg, Prog. Inorg. Chem. **12,** 295 (1970).
[3] L. Alcàcer and H. Novais, in: Extended Linear Chain Compounds (J. S. Miller, ed.). Plenum Press, New York 1982, 3, Chapter 6.
[4] S. Alvarez, R. Vicente, and R. Hoffmann, J. Amer. Chem. Soc. **107,** 6253 (1985).
[5] S. I. Shupack, E. Billig, R. J. H. Clark, R. Williams, and H. B. Gray, J. Amer. Chem. Soc. **86,** 4594 (1964).
[6] D. M. Adams and J. B. Cornell, J. Chem. Soc. (A), **1968,** p. 1299.
[7] C. W. Schläpfer and K. Nakamoto, Inorg. Chem. **14,** 1338 (1975).
[8] R. J. H. Clark and P. C. Turtle, J. Chem. Soc., Dalton Trans. **1977,** p. 2142.
[9] S. O. Grim, L. J. Matienzo, and W. E. Swartz, Inorg. Chem. **13,** 447 (1974).
[10] R. D. Schmitt and A. H. Maki, J. Amer. Chem. Soc. **90,** 2288 (1968).
[11] R. Kirmse and W. Dietzsch, J. Inorg. Nucl. Chem. **38,** 255 (1976).
[12] R. Kirmse, W. Dietzsch, and B. V. Solov'ev, J. Inorg. Nucl. Chem. **39,** 1157 (1977).
[13] W. E. Geiger, jr., C. S. Allen, T. E. Mines, and F. C. Senftleber, Inorg. Chem. **16,** 2003 (1977).
[14] W. Güntner, U. Klement, M. Zabel, and G. Gliemann, Inorg. Chim. Acta, in press.
[15] W. Güntner and G. Gliemann, J. Phys. Chem., in press.
[16] C. E. Johnson, R. Eisenberg, T. R. Evans, and M. S. Burberry, J. Amer. Chem. Soc. **105,** 1795 (1983).
[17] P. Bradley, Thesis, Rochester, New York 1987.
[18] I. Hidvegi, W. v. Ammon, and G. Gliemann, J. Chem. Phys. **76,** 4361 (1982).
[19] W. v. Ammon and G. Gliemann, J. Chem. Phys. **77,** 2266 (1982).
[20] W. Tuszynski and G. Gliemann, Ber. Bunsenges. Phys. Chem. **89,** 940 (1985).
[21] E. G. Megehee, C. E. Johnson, and R. Eisenberg, to be published.
[22] G. N. Schrauzer and V. P. Mayweg, J. Amer. Chem. Soc. **20,** 3586 (1965).